Research Article

Xi Nan, Tomotaka Hatakeyama, Shuntaro Ida, Nobuaki Sekido, and Kyosuke Yoshimi*

Effect of Cr and Al alloying on the oxidation resistance of a Ti_5Si_3-incorporated MoSiBTiC alloy

https://doi.org/10.1515/htmp-2021-0024
received January 05, 2021; accepted April 14, 2021

Abstract: The effects of adding Cr and Al on the oxidation behavior of a Ti_5Si_3-incorporated MoSiBTiC alloy (46Mo–28Ti–14Si–6C–6B, at%) were investigated at 800 and 1,100°C. The addition of Cr and Al largely improved the oxidation resistance of the MoSiBTiC alloy at 800°C due to the formation of $Cr_2(MoO_4)_3$ and $Al_2(MoO_4)_3$ in the oxide scales. These protective molybdates mainly formed on the molybdenum solid solution (Mo_{ss}) and Mo_3Si phases that show poor oxidation resistance in the Cr- and Al-free alloy and consequently increased the oxidation resistance of the alloys. However, accelerated oxidation occurred on the 10Al alloy after the long-term oxidation test, suggesting that the formed oxide scale has limited protection ability. At 1,100°C, the addition of Cr and Al also enhanced the oxidation resistance to some extent by forming Cr_2O_3 and Al_2O_3 in the oxide scales.

Keywords: molybdenum, oxidation resistance, high-temperature materials, chromium addition, aluminum addition

1 Introduction

Molybdenum–silicon–boron (Mo–Si–B) alloys are promising ultra-high temperature structural materials for heat engines because of their high melting point and impressive creep strength above 1,150°C [1–5]. Nevertheless, the poor room-temperature fracture toughness and inadequate oxidation resistance of Mo–Si–B alloys prevent their practical use [5–7]. Recently, Moriyama et al. found that a TiC-added Mo–Si–B alloy with a typical composition of 65Mo–10Ti–5Si–10C–10B (at%, so-called first-generation MoSiBTiC alloy) showed improved room-temperature fracture toughness compared with conventional Mo–Si–B ternary alloys [8]. The density of this alloy has also been reduced by TiC addition to 8.9 g/cm^3 [9], which is within the range of nickel-based single-crystal superalloys. Kamata et al. further revealed that this alloy possessed excellent creep strength (a rupture time of ~400 h at 1,400°C under 137 MPa) [10]. However, the oxidation resistance of the first-generation MoSiBTiC alloy is very poor, mainly due to the relatively low concentration of Si and the large volume fraction of the molybdenum solid solution (Mo_{ss}) phase [11]. Experimental efforts to solve this problem by incorporating Ti_5Si_3, an oxidation-resistant intermetallic phase, into MoSiBTiC alloy have been attempted. The composition modified as a Ti_5Si_3-incorporated MoSiBTiC alloy is 46Mo–28Ti–14Si–6C–6B (at%), which exhibited better oxidation performance than the first-generation MoSiBTiC alloy at 1,100°C [12]. Unfortunately, due to the low protection from the boron-containing silicate formed at intermediate temperature, a remarkable weight loss of the 46Mo–28Ti–14Si–6C–6B alloy upon exposure to oxygen was observed at 800°C [12,13].

It is well known that Cr and Al are beneficial alloying elements for improving oxidation resistance by forming protective Cr_2O_3 and Al_2O_3 layers. The effects of Cr in Mo–Si–B alloys were investigated by Burk et al. [14]. The Mo–Si–B–Cr alloys showed increased oxidation resistance with the increasing Cr content from 5 to 25 at%. A fully passivated $Cr_2(MoO_4)_3$ layer was formed on the Mo–9Si–8B–25Cr alloy oxidized at 750°C for 10 h. Ström et al. also reported the formation of $Cr_2(MoO_4)_3$ on the Cr-alloyed $MoSi_2$ at 450°C [15]. Alloying with Al was proved to be able to suppress the pest phenomenon and thus enhanced the oxidation behavior of Mo–Si alloys due to

* **Corresponding author: Kyosuke Yoshimi,** Department of Materials Science, Graduate School of Engineering, Tohoku University, Sendai, 980-8579, Japan, e-mail: yoshimi@material.tohoku.ac.jp
Xi Nan, Shuntaro Ida, Nobuaki Sekido: Department of Materials Science, Graduate School of Engineering, Tohoku University, Sendai, 980-8579, Japan
Tomotaka Hatakeyama: International Center for Young Scientists (ICYS), National Institute for Materials Science (NIMS), 1-2-1 Sengen, Tsukuba, Ibaraki, 305-0047, Japan

the presence of the Al_2O_3 scale on the surface at high temperature [16–19]. Zhao et al. also reported that adding Al or Cr into Mo–Ti–Si–B alloy (35Mo–35Ti–20Si–10B) yielded better intermediate-temperature oxidation resistance [20].

Therefore, in the present study, varying amounts of Cr and Al were added to the Ti_5Si_3-incorporated MoSiBTiC alloy, and the oxidation performance was evaluated by analyzing oxidation kinetic curves and oxide scales formed at different temperatures, aiming to provide insights for the alloy design of advanced MoSiBTiC alloys for ultra-high temperature applications.

2 Experimental procedures

The Cr- and Al-added Ti_5Si_3-incorporated MoSiBTiC alloys investigated in this study have the compositions of 36Mo–28Ti–14Si–6C–6B–(10–x)Cr–xAl (x = 0, 5 and 10, at%). For simplicity, they are denoted as base (46Mo and no Cr and Al), 10Cr, 5Cr5Al and 10Al alloys, respectively. These alloys were prepared by conventional arc-melting with a water-cooled copper crucible from high-purity Mo (99.9%), Ti (99.995%), Si (99.99%), Cr (99.9%), Al (99.99%), MoB (99%) and cold-pressed TiC powder (99 wt%, 2–5 μm in diameter) under an argon atmosphere. The button ingots were flipped over and remelted five times to ensure compositional homogenization. Heat treatment was performed at 1,600°C for 10 h under an argon atmosphere. There was no noticeable weight change of the ingots before and after heat treatment. The chemical compositions of the investigated Ti_5Si_3-incorporated MoSiBTiC alloys are summarized in Table 1. In particular, boron was measured using inductively coupled plasma analysis.

A Bruker D8 Advance X-ray diffractometer (XRD) with Cu-Kα radiation was used for phase identification. The data were collected over a 2θ range of 20–80° with a step size of 0.02° and a count time of 0.5 s/step. Microstructure characterization was conducted using a JEOL JSM-7800F scanning electron microscope (SEM) in a backscattered electron imaging mode. Chemical analysis of constituent phases for Mo, Ti, Si, Cr and Al were carried out using energy-dispersive X-ray spectroscopy (EDX) and electron probe micro analyzer (EPMA) on a JEOL JCM 6000PLUS microscope. B and C were neglected during the measurements due to the serious interference problem between the characteristic lines of Mo and B as well as the low quantitative capability of EDX for these light elements.

For oxidation studies, coupon specimens were sliced from the heat-treated ingots by electron-discharge machining. These specimens were carefully polished using 2000-grit SiC paper to fully remove the heat-damaged layers and given final dimensions of approximately $4 \times 3 \times 0.5\,mm^3$. They were then cleaned ultrasonically in ethanol for 30 min and dried in air. Oxidation tests were performed isothermally at 800°C for 50 h and 1,100°C for 12 h under an Ar–21% O_2 gas flow using a Shimadzu TGA-50H thermogravimetric analyzer. The weight change of the specimens was continuously recorded against time to acquire oxidation kinetic curves. The oxidized specimens were also carefully examined by XRD, SEM, EDX and EPMA.

3 Results and discussion

3.1 Microstructure

Figure 1 shows the microstructures of the (a) base, (b) 10Cr, (c) 5Cr5Al and (d) 10Al alloys after 1,600°C/10 h heat treatment. As shown in Figure 1(a) and (b), the base and 10Cr alloys had the same phase constitution, that is, Mo_{ss}, Ti_5Si_3, Mo_5SiB_2 (T_2) and TiC. It is suggested that the addition of Cr did not change the phase equilibrium of the base alloy. However, the microstructure of the 10Cr alloys was much coarser than that of the base alloy. Mo_3Si was detected in the 5Cr5Al and 10Al alloys, accompanying the decreased volume fraction of Mo_{ss} (see Figure 1(c) and (d)). In the 10Al alloy, only the polygonal prism-shaped Ti_5Si_3 rods elongating along the solidification direction can be seen, and the fine secondary Ti_5Si_3 as observed in the eutectic regions of the base alloy almost disappeared. Some spheroidized Mo_3Si particles

Table 1: Chemical compositions of the investigated Ti_5Si_3-incorporated MoSiBTiC alloys (at%)

Alloy	Mo	Ti	Si	C	B	Cr	Al
Base	46.4 ± 1.1	28.4 ± 0.6	13.0 ± 1.2	5.9 ± 0.6	6.1 ± 0.3	<0.1	<0.1
10Cr	37.1 ± 1.4	28.8 ± 1.1	13.1 ± 1.9	6.3 ± 0.8	5.6 ± 0.5	9.0 ± 1.2	<0.1
5Cr5Al	37.2 ± 1.5	29.1 ± 2.0	13.1 ± 0.9	6.2 ± 0.5	5.5 ± 0.7	4.6 ± 0.9	4.3 ± 1.0
10Al	37.0 ± 1.2	28.8 ± 1.5	13.3 ± 1.3	6.1 ± 0.4	5.7 ± 0.60	<0.1	9.0 ± 1.4

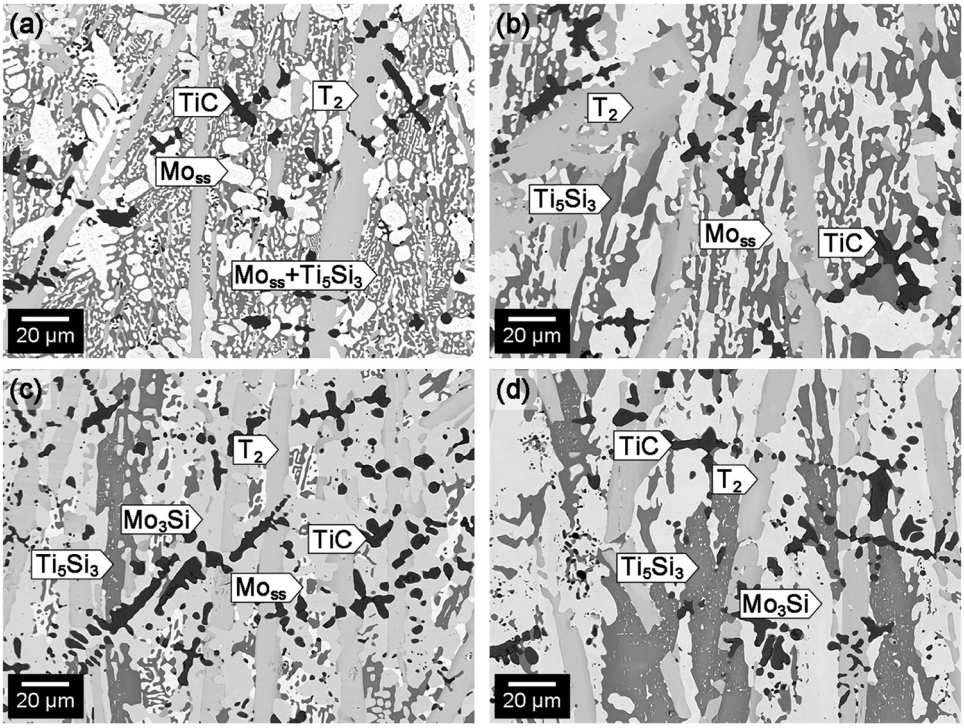

Figure 1: Microstructures of the heat-treated (a) base, (b) 10Cr, (c) 5Cr5Al and (d) 10Al alloys.

precipitated in the polygonal prism-shaped Ti_5Si_3 of the Al-added alloys during annealing. The compositions of each constituent phase measured by SEM-EDX for the heat-treated alloys are presented in Table 2. A large amount of Ti was dissolved in Mo_{ss} (~20 at%), Mo_3Si (~23 at%) and T_2 (~31 at%), while a large amount of Mo was dissolved in Ti_5Si_3 (~20 at%) and TiC (~9 at%). In the Cr-added alloys, Cr mainly dissolved in Mo_{ss} and Mo_3Si phases. The previous work by Hatakeyama et al. revealed that Cr can substitute at Mo sites in the Mo_{ss} and T_2 phases and barely change the constituent phases of the alloy [12]. Al mainly dissolved in the Mo_3Si phases in Al-added alloys because Al is a $Mo_3(Si,Al)$-forming element [16,21]. In addition, the concentrations of both Cr and Al in TiC phase are negligible (less than 1%). Figure 2 presents the volume fractions of phase constituents in the heat-treated alloys. The volume fraction of T_2 and TiC phases also showed insignificant changes with the addition of Cr and Al.

3.2 Oxidation behavior at 800°C

Figure 3(a) illustrates the isothermal oxidation curves of the alloys obtained at 800°C. The base alloy showed a rapid weight loss (–60 mg/cm^2 for 5 h) correlating with the evaporation of MoO_3, B_2O_3 and CO_2 from the oxidized surfaces [22–24]. In contrast, the 10Cr, 5Cr5Al and 10Al alloys exhibited dramatically reduced weight losses upon oxidation exposure. The weight changes of the 10Cr and 5Cr5Al alloys after 50 h oxidation were less than –1 mg/cm^2. This indicates that the weight loss of the base alloy at 800°C can be suppressed by adding Cr and/or Al. It is noteworthy that the weight loss rate of the 10Al alloy suddenly increased from ~22 h of oxidation. The appearances of the specimens oxidized for 50 h are shown in Figure 3(b)–(e). After the 12 h oxidation test, the base alloy did not change in shape and appeared intact (Figure 3(b)). The 10Cr and 5Cr5Al specimens showed no spalling or cracking after the 50 h oxidation tests, as shown in Figure 3(c) and (d). Nevertheless, the edges of the 10Al coupon became distorted after the oxidation test (Figure 3(e)). This may be related to the suddenly accelerated oxidation as seen in the kinetic curve.

Figure 4 shows the XRD spectra of the base and Cr/Al-added alloy samples after 50 h oxidation at 800°C. TiO_2 reflections were detected in all samples. Characteristic reflections of chromium and aluminum molybdates ($X_2(MoO_4)_3$, X = Cr or/and Al) were observed in the Cr/Al-added alloys. In addition, some weak Al_2O_3 reflections were also detected in the 10Al alloy. Noteworthy is that signals from MoO_3, which should have evaporated during oxidation are also present in the XRD spectra. It might be related to the desublimation of MoO_3 during cooling. The

Table 2: Compositions of each constituent phase as measured by SEM-EDX for the heat-treated alloys (at%)

	10Cr alloy				5Cr5Al alloy				10Al alloy			
	Mo_{ss}	Ti_5Si_3	T_2	TiC	Mo_{ss}	Mo_3Si	Ti_5Si_3	T_2	TiC	Mo_3Si	Ti_5Si_3	T_2	TiC
Mo	61.2 ± 2.2	18.6 ± 1.5	47.0 ± 3.6	8.6 ± 2.1	63.5 ± 3.4	50.2 ± 1.1	18.8 ± 2.2	50.6 ± 1.6	8.4 ± 1.1	56.9 ± 2.3	23.1 ± 0.9	54.5 ± 2.8	9.7 ± 0.4
Si	2.4 ± 0.8	31.7 ± 0.9	14.0 ± 1.1	0.4 ± 0.1	1.6 ± 0.6	12.7 ± 0.4	30.2 ± 1.2	14.1 ± 0.4	0.2 ± 0.1	9.8 ± 0.7	27.3 ± 0.6	13.8 ± 0.3	0.2 ± 0.1
Ti	19.2 ± 1.1	44.0 ± 1.9	32.6 ± 2.6	90.8 ± 2.7	21.4 ± 1.1	23.5 ± 0.5	44.7 ± 2.0	31.7 ± 1.7	90.5 ± 1.0	22.0 ± 1.4	44.5 ± 1.5	30.5 ± 2.7	89.3 ± 0.9
Cr	17.2 ± 1.0	5.7 ± 0.6	6.4 ± 0.4	0.2 ± 0.2	8.7 ± 0.7	6.9 ± 0.5	3.0 ± 0.3	2.6 ± 0.4	0.3 ± 0.1	—	—	—	—
Al	—	—	—	—	4.8 ± 0.4	6.7 ± 0.6	3.3 ± 0.2	1.0 ± 0.2	0.6 ± 0.1	11.3 ± 0.3	5.1 ± 1.1	1.2 ± 0.2	0.8 ± 0.2

cross-section microstructures of all the alloys oxidized at 800°C for 50 h are shown in Figure 5, with the oxide scales identified by XRD and EPMA analyses as described in this article. As shown in Figure 5(a), the base alloy specimen was completely oxidized, and its oxide scale was composed of TiO_2, SiO_2 and unoxidized Ti_5Si_3. Even though no SiO_2 signals were detected by XRD, high Si and O concentrations measured by EPMA from the oxide scale (15.5Ti–17.2Si–67.3O, at%) could prove the formation of SiO_2. The poor oxidation resistance of the base alloy at 800°C is mainly attributed to the rapid oxidation of the Mo_{ss} phase and the resultant sublimation of MoO_3. Although the Ti_5Si_3 phase possesses good oxidation resistance and barely oxidizes at 800°C [25,26], it cannot form a protective scale covering the entire specimen due to the small amount of oxidation products. Therefore, the oxidation proceeded along the continuous Mo_{ss} phase to form a microporous TiO_2/SiO_2 scale. Detailed analyses of the oxidation behavior of the base alloy have been reported elsewhere [13,27]. The oxide scales formed on the 10Cr, 5Cr5Al and 10Al specimens after oxidation for 50 h were very thin (average thickness less than 15 μm). The Ti_5Si_3 phase in each alloy also barely oxidized and exhibited significant oxidation resistance among constituent phases. Particularly, the recession depths of Mo_{ss} and Mo_3Si phases reduced to less than 6 μm in contrast to the preferentially oxidized Mo_{ss} phase in the base alloy. For the 10Cr alloy, the oxide scale was composed of TiO_2, SiO_2 and $Cr_2(MoO_4)_3$ (see Figure 5(b)). The molybdate was mainly distributed on the Mo_{ss} phase due to the high amount of Cr dissolved in Mo_{ss} (~15 at%) and acted as a protective barrier, which prevented further oxidation. This agrees with the result reported by Burk et al. that the $Cr_2(MoO_4)_3$ layer formed on the Mo–9Si–8B–25Cr alloy oxidized at 750°C is fully passivated [14]. In the scale formed on the 5Cr5Al specimen, the molybdate $(Cr,Al)_2(MoO_4)_3$ was also detected.

Figure 6 shows EPMA elemental maps of the oxidized 5Cr5Al alloy specimen. It was found that Ti spread over the whole oxide scale, and Si was mainly distributed in the scale upon the silicide phases. An internal oxidation region, which formed on the top of the T_2 phase (indicated by a thick arrow), was Ti and Si deficient, containing a detectable concentration of Mo and O (see Figure 6(f) and (g)). This internal oxidation region formed on the T_2 phase was reported elsewhere [6]. The distributions of Cr and Mo were quite uniform (indicated by thin arrows in Figure 6(d)–(f)), and Al also existed in these Cr/Mo-rich regions, coinciding with the molybdate mainly formed on the Mo_{ss} and Mo_3Si. This agrees with the portioning behavior of Cr and Al in each constituent phase as

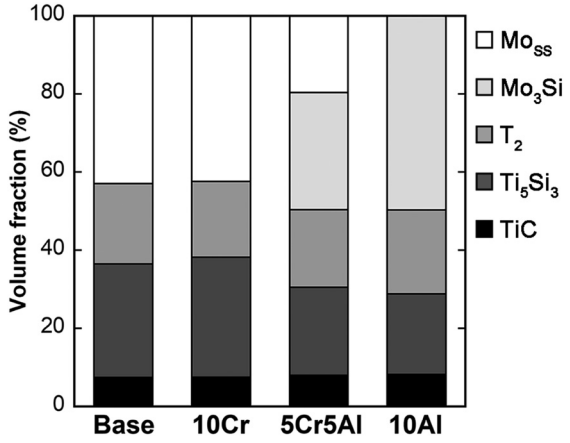

Figure 2: Volume fractions of constituent phases of the heat-treated alloys.

presented in Table 2. Moreover, a high Al content was observed at the outermost layer of the oxide scale, indicating the formation of Al_2O_3. Similar outward diffusion of Al had been reported for Ti–Al–Si alloys [28,29]. The oxide scale formed on the 10Al specimen had similar oxide scales to that of the 5Cr5Al alloy (see Figure 5(d)). However, the discontinuous Al_2O_3 layer formed on the outermost scale could not provide sufficient protection for the substrate. It can be concluded that the addition of Cr and Al to the base alloy contributed to the formation of protective molybdates upon Mo_{ss} and Mo_3Si phases, which suppressed the inward diffusion of oxygen and consequently increased the oxidation resistance of the entire alloy.

Even though these chromium and aluminum molybdates, which formed at and below 800°C on the MoSiBTiC alloys, acted as protective oxide, $Cr_2(MoO_4)_3$ and $Al_2(MoO_4)_3$ decompose with MoO_3 vaporization at temperatures starting from 810 and 800°C, respectively [30,31]. Since the decomposition temperature of $Al_2(MoO_4)_3$ is the same as the oxidation temperature in this study, the formation and decomposition of $Al_2(MoO_4)_3$ may progress simultaneously during the oxidation process. This agrees with the SEM results that both $Al_2(MoO_4)_3$ and Al_2O_3 were observed in the Al-added alloys (see Figure 5(d)). Therefore, for the 10Al alloy that showed good oxidation resistance in the first several hours (shown in Figure 3(a)), the accelerated oxidation from ~22 h and the distorted sample edges (see Figure 3(e)) were presumably due to the decomposition of $Al_2(MoO_4)_3$ to Al_2O_3 and volatile MoO_3 after the long-term oxidation test.

3.3 Oxidation behavior at 1,100°C

Figure 7 shows the isothermal oxidation curves of the alloys at 1,100°C and the appearance of the specimens after 12 h of oxidation. The weight loss corresponds to the evaporation of MoO_3, B_2O_3 and CO_2 during oxidation. As shown in Figure 7(a), all of the alloys experienced a rapid weight loss at the beginning of the oxidation (called the "initial stage"), followed by a gradual slowing down of the oxidation rate. Compared with the base alloy for which the initial stage ended around 1 h, the 10Cr, 5Cr5Al and 10Al alloys exhibited a shorter initial stage with the ending time around 10 min. The weight loss in the initial stages of the 10Cr, 5Cr5Al and 10Al alloys was much smaller than that of the base alloy. However, all the alloys

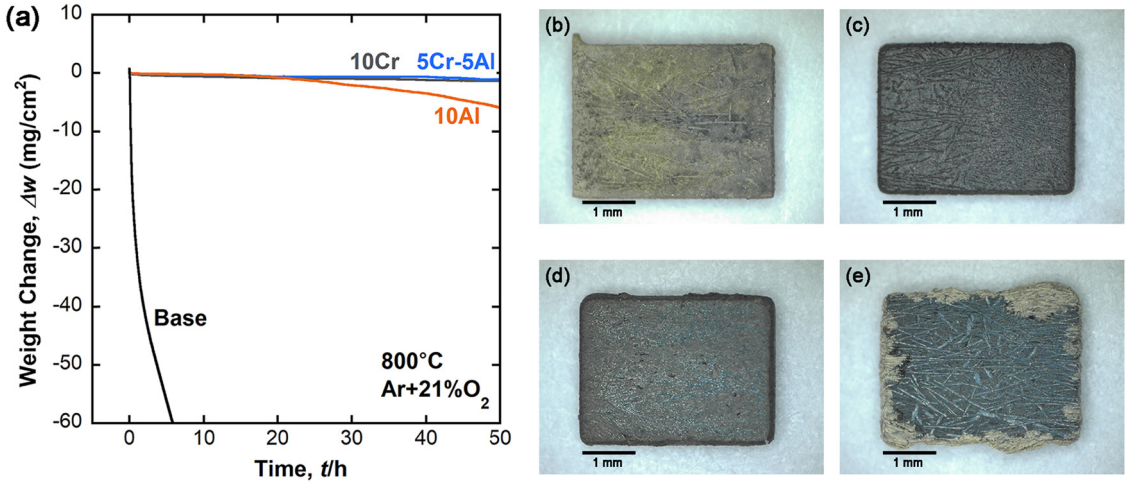

Figure 3: (a) Isothermal oxidation curves of the alloys obtained at 800°C and appearances of the specimens of the (b) base, (c) 10Cr, (d) 5Cr5Al and (e) 10Al alloys oxidized for 50 h.

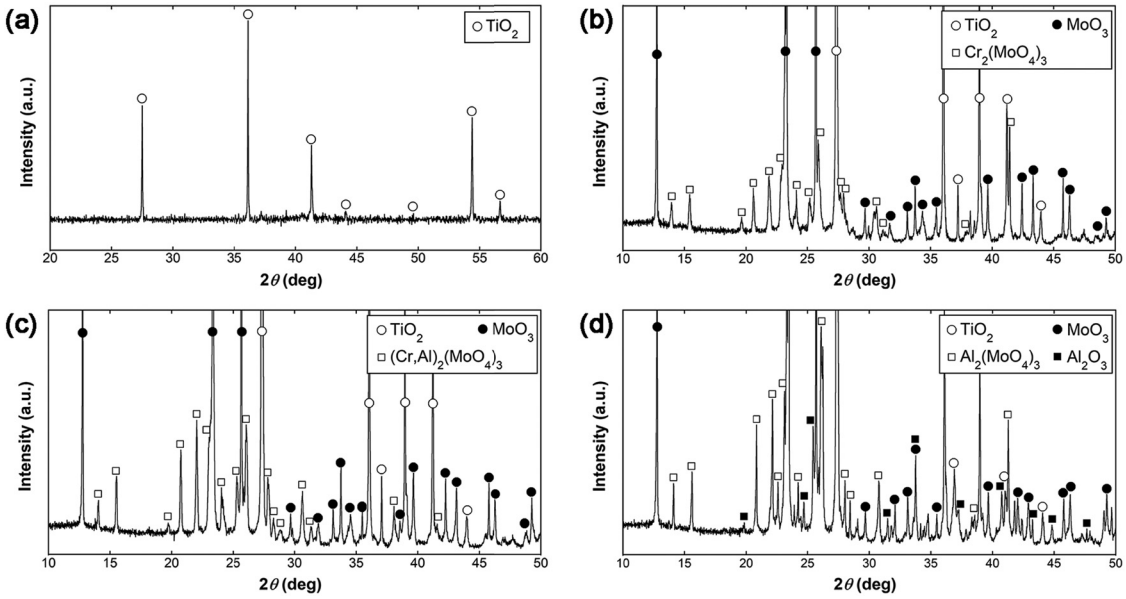

Figure 4: XRD spectra of the (a) base, (b) 10Cr, (c) 5Cr5Al and (d) 10Al alloys after 50 h oxidation at 800°C.

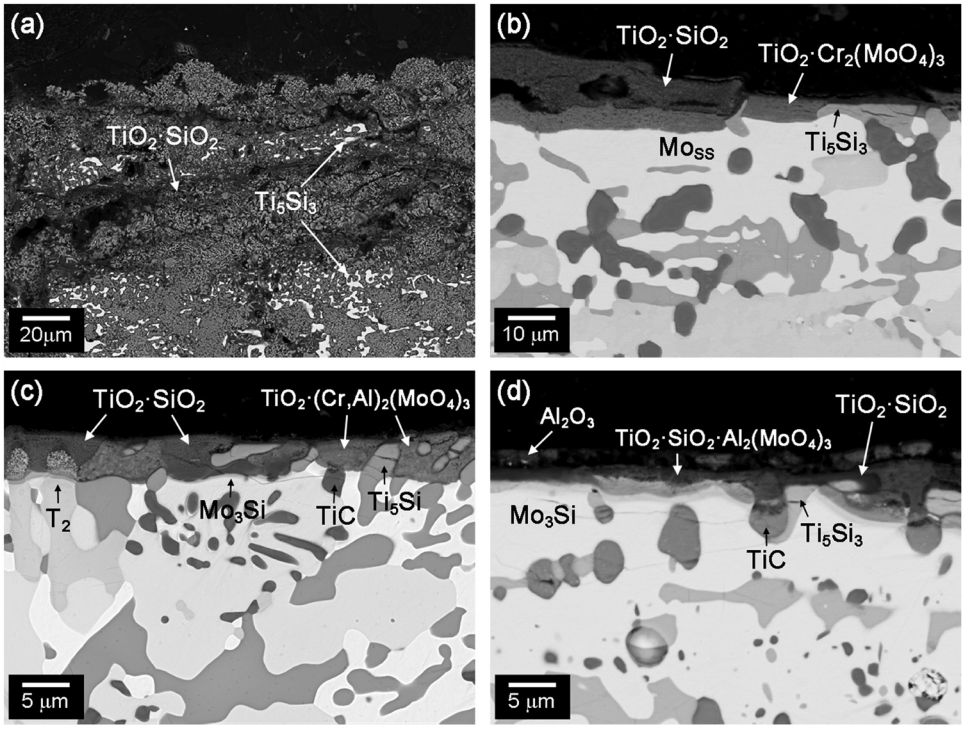

Figure 5: Cross-section microstructures of the (a) base, (b) 10Cr, (c) 5Cr5Al and (d) 10Al alloys oxidized at 800°C for 50 h.

showed a continuous weight loss in a linear manner after the initial stage. This means that the oxide scales, which formed on the substrates did not completely passivate them, and thus, the sublimation of MoO_3 could not be fully suppressed. Figure 7(b)–(e) show the appearance of the alloys oxidized at 1,100°C for 12 h. It can be seen that the

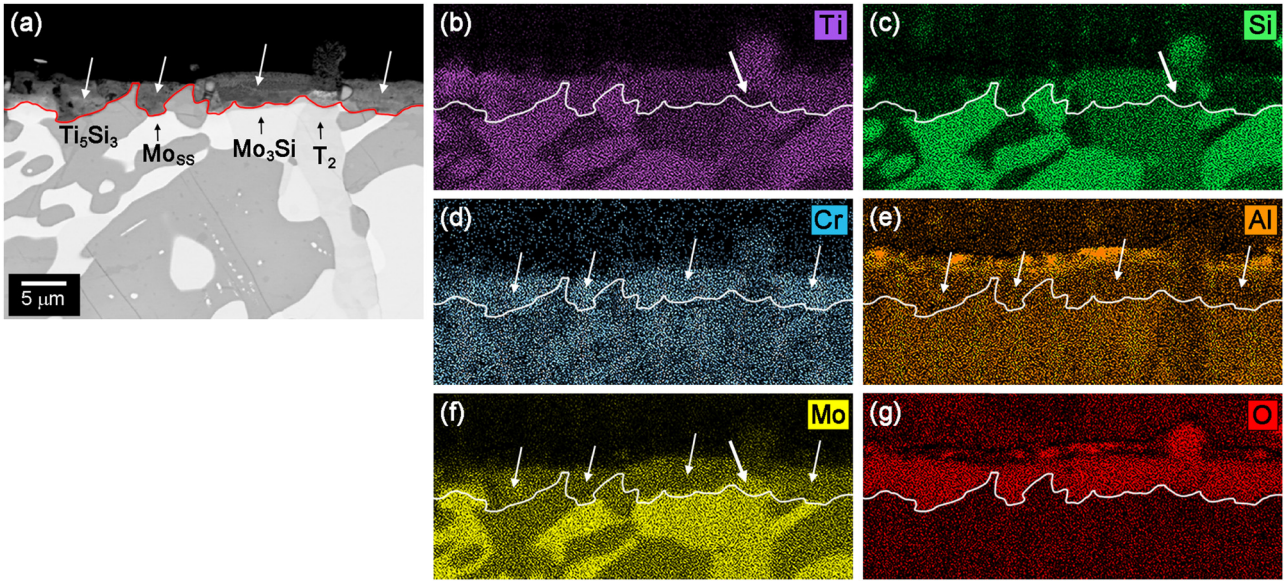

Figure 6: (a) Cross-section BSE image and (b)–(g) the corresponding EPMA elemental maps of the 5Cr5Al alloy oxidized at 800°C for 50 h.

base alloy contained some protruded oxides along the specimen edges (see Figure 7(b)). In contrast, the Cr/Al-added alloys had neat surface morphology as shown in Figure 7(c)–(e). Figure 8 shows the XRD patterns obtained from the surface of the base and Cr/Al-added alloys oxidized at 1,100°C for 12 h. Strong TiO_2 reflections were detected, indicating that the main component of the oxide scale was rutile TiO_2. The 10Cr alloy had a similar XRD pattern with the base alloy, with only TiO_2 being detected. For the Al-added alloys, Al_2O_3 formed in the scales during the oxidation test, coinciding with the color change of the sample surfaces shown in Figure 7(c) and (d).

The cross-section microstructures of the base, 10Cr, 5Cr5Al and 10Al alloys oxidized at 1,100°C for 12 h are shown in Figure 9(a)–(e). The average scale thickness of the base, 10Cr, 5Cr5Al and 10Al alloys was 40, 30, 30 and 32 μm, respectively. SiO_2 was detected in the oxide layers by EPMA analysis even though there were no silicate peaks in the XRD patterns. The oxide scale formed in the 10Cr alloy was mainly composed of TiO_2 and SiO_2 as shown in Figure 9(b). Meanwhile, as shown in Figure 9(c), some light gray particles mainly distributed near the scale/substrate interface can be seen for the 10Cr alloy. The results of EPMA analysis listed in Table 3 show that

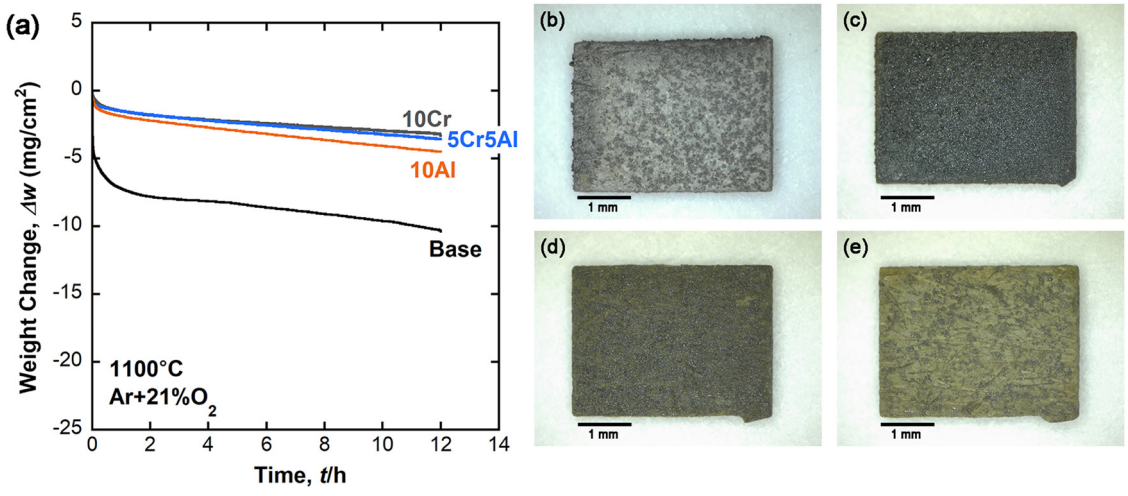

Figure 7: (a) Isothermal oxidation curves of the alloys obtained at 1,100°C and the appearance of the (b) base, (c) 10Cr, (d) 5Cr5Al and (e) 10Al specimens oxidized for 12 h.

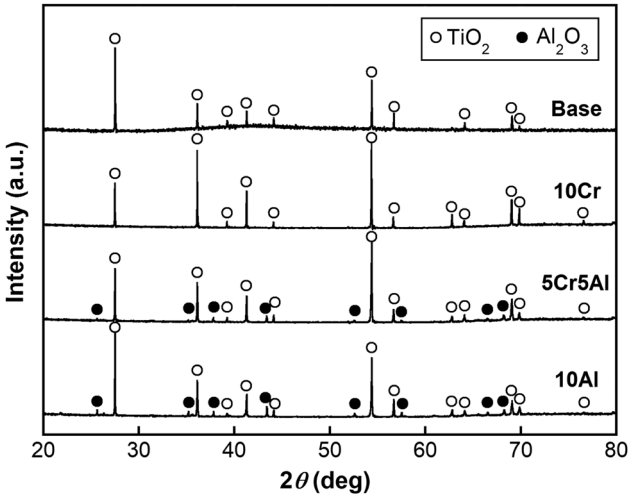

Figure 8: XRD spectra of the specimen surface of the base, 10Cr, 5Cr5Al and 10Al alloys oxidized at 1,100°C for 12 h.

the light gray particles should be Cr_2O_3. Figure 10 shows an (a) cross-section BSE image with the corresponding EDX elemental maps illustrated the 10Cr alloy oxidized at 1,100°C for 12 h in (b)–(f). High Ti and Si contents were observed in the oxide scale. Cr tended to concentrate on the inner side of the scale (see Figure 10(e)), coinciding with the Cr_2O_3 particles that are shown in Figure 9(c). The formation of Cr_2O_3 suppressed the inward diffusion of oxygen at some depth, thereby increasing the oxidation

Table 3: Composition of the light gray phase in the oxide scale in Figure 9(c) (at%)

Element	Content
Mo	1.2 ± 0.3
Ti	5.4 ± 1.3
Si	1.9 ± 0.1
Cr	29.5 ± 2.7
O	62.0 ± 7.2

resistance at high temperature. No Cr_2O_3 particles were detected in the scale near the surface from the XRD or SEM results, where a detectable Cr concentration was found. The absence of Cr_2O_3 particles near the scale/gas interface may be due to the lower oxygen affinity of Cr than Ti, which suppressed the Cr_2O_3 formation at the beginning of oxidation or by the sublimation of volatile CrO_3 from the scale surface [32]. The oxide scale formed on the 5Cr5Al and 10Al specimens was composed of a TiO_2/Al_2O_3 outermost layer and a TiO_2/SiO_2 inner layer. Cr_2O_3 particles were also observed in the scale of the oxidized 5Cr5Al specimen. Since Al has a high affinity with oxygen, Al_2O_3 would form preferentially at the very beginning of oxidation. However, the Al concentration in the 5Cr5Al and 10Al alloys was relatively low compared with the Ti concentration. Once Al diffused to the surface, the lean-Al region underneath allowed Ti to oxidize to

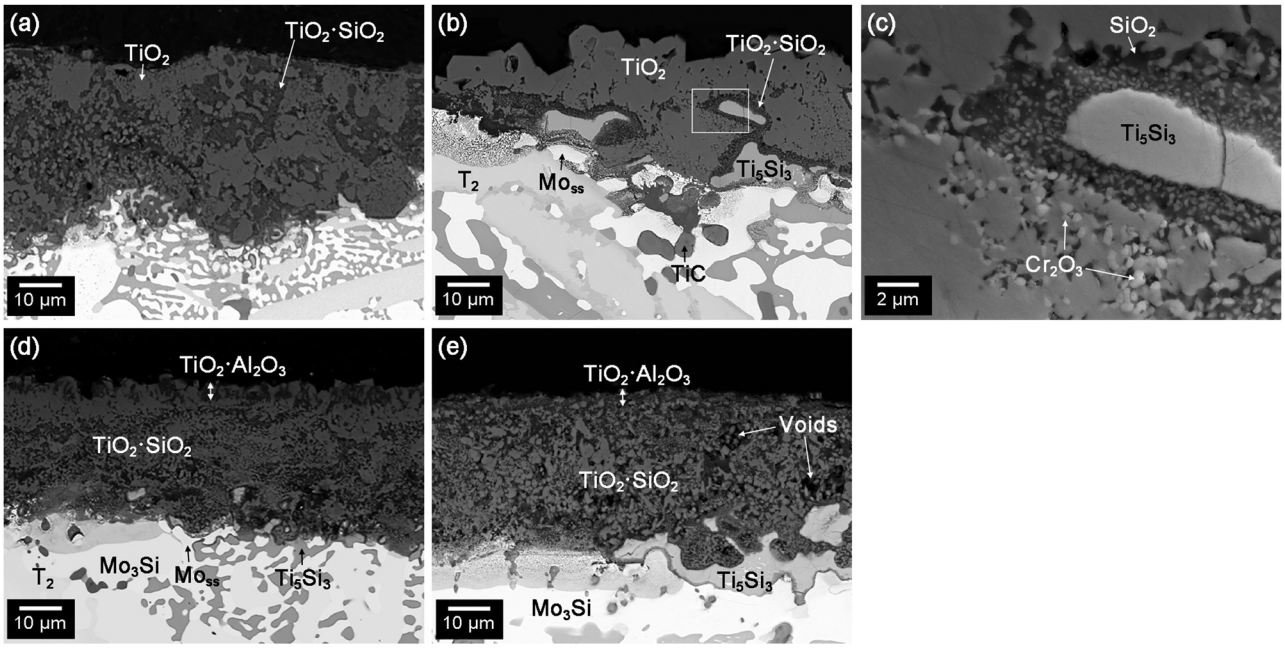

Figure 9: Cross-section microstructures of the (a) base, (b) 10Cr, (d) 5Cr5Al and (e) 10Al alloys oxidized at 1,100°C for 12 h, (c) high magnification image of the squared area in (b).

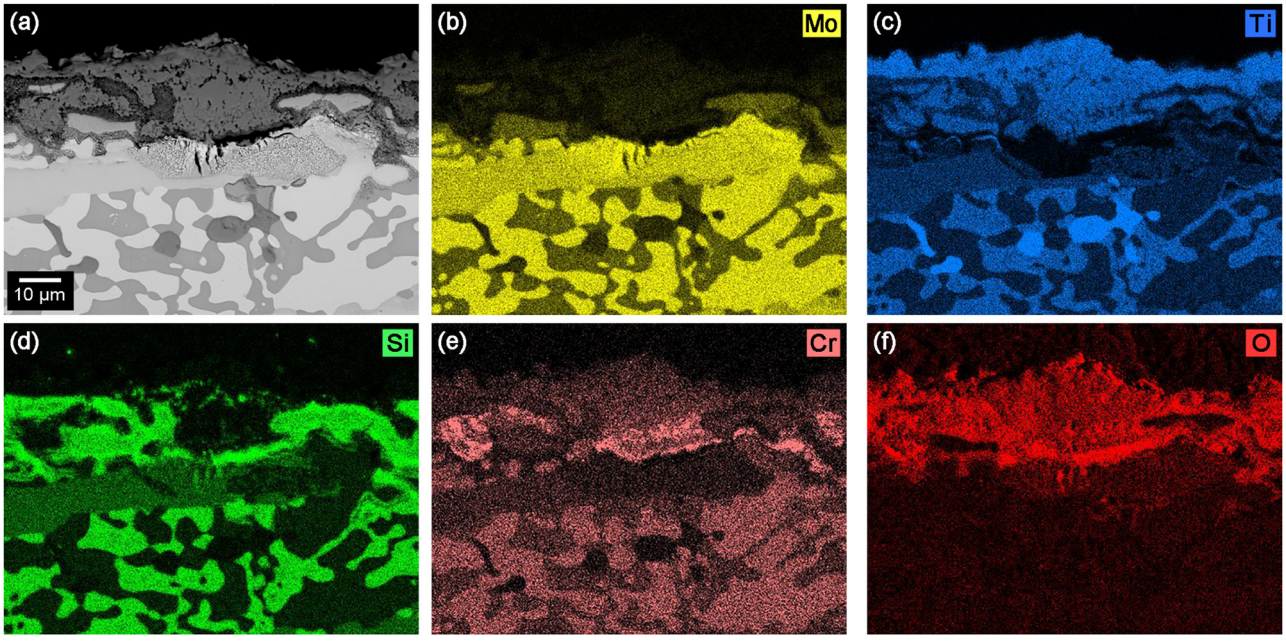

Figure 10: (a) Cross-section BSE image and (b)–(f) the corresponding EDX elemental maps of the 10Cr alloy oxidized at 1,100°C for 12 h.

TiO_2, giving rise to a mixed outermost layer composed of TiO_2 and Al_2O_3 instead of the continuous alumina layer. This oxide scale structure was similar to the scale formed on the Ti–Al-based alloys with relatively low Al content [28,33,34]. In contrast to the oxide scale of the 10Cr alloy, which consisted of coarse TiO_2 grains, these Al_2O_3-containing scales showed very fine oxide grains. Together with voids as shown in Figure 9(e), these Al_2O_3-containing scales likely offer only limited protection even though Al_2O_3 is considered to be an oxidation-resistant phase in many alloy systems.

4 Conclusion

The effects of adding Cr and Al on the oxidation behavior of a Ti_5Si_3-incorporated MoSiBTiC alloy were investigated. The addition of Cr did not change the constituent phases of the base alloy but coarsened the microstructure, while Mo_3Si phases formed by Al alloying. Compared with the base alloy, the alloys added with Cr and Al exhibited largely improved oxidation resistance at 800°C due to the formation of protective $Cr_2(MoO_4)_3$ and $Al_2(MoO_4)_3$. These molybdates mainly formed upon Mo_{ss} and Mo_3Si phases that showed poor oxidation resistance in the base alloy and consequently increased the oxidation resistance of the alloys. However, accelerated oxidation occurred on the 10Al alloys after the long-term oxidation test, indicating that the formed oxide scale has limited protection ability. At 1,100°C, the addition of Cr and Al also enhanced the oxidation resistance to some extent by forming Cr_2O_3 and Al_2O_3 in the oxide scales.

Acknowledgments: This research was partly supported by the Japan Science and Technology (JST)–Mirai Program (Grant Number JPMJMI17E7).

Funding information: This research was partly supported by the Japan Science and Technology (JST)–Mirai Program (Grant Number JPMJMI17E7).

Author contributions: Xi Nan: writing – original draft, conceptualization, methodology, investigation; Tomotaka Hatakeyama: conceptualization; Shuntaro Ida: writing – review and editing; Nobuaki Sekido: writing – review and editing; Kyosuke Yoshimi: resource, supervision, project administration.

Conflict of interest: The authors state no conflict of interest.

References

[1] Pollock, T. M. Alloy design for aircraft engines. *Nature Materials*, Vol. 15, No. 8, 2016, pp. 809–815.
[2] Perepezko, J. H. The hotter the engine, the better. *Science*, Vol. 326, No. 5956, 2009, pp. 1068–1069.

[3] Jain, P. and K. S. Kumar. Tensile creep of Mo–Si–B alloys. *Acta Materialia*, Vol. 58, No. 6, 2010, pp. 2124–2142.
[4] Zhang, W., P. K. Liaw, and Y. Zhang. Science and technology in high-entropy alloys. *Science China Materials*, Vol. 61, 2018, pp. 2–22.
[5] Lemberg, J. A. and R. O. Ritchie. Mo–Si–B alloys for ultrahigh-temperature structural applications. *Advanced Materials*, Vol. 24, No. 26, 2012, pp. 3445–3480.
[6] Yoshimi, K., S. Nakatani, T. Suda, S. Hanada, and H. Habazaki. Oxidation behavior of Mo_5SiB_2-based alloy at elevated temperatures. *Intermetallics*, Vol. 10, No. 5, 2002, pp. 407–414.
[7] Parthasarathy, T. A., M. G. Mendiratta, and D. M. Dimiduk. Oxidation mechanisms in Mo–reinforced $Mo_5SiB_2(T_2)$–Mo_3Si alloys. *Acta Materialia*, Vol. 50, No. 7, 2002, pp. 1857–1868.
[8] Moriyama, T., K. Yoshimi, M. Zhao, T. Masnou, T. Yokoyama, J. Nakamura, et al. Room-temperature fracture toughness of MoSiBTiC alloys. *Intermetallics*, Vol. 84, 2017, pp. 92–102.
[9] Miyamoto, S., K. Yoshimi, S. H. Ha, T. Kaneko, J. Nakamura, T. Sato, et al. Phase equilibria, microstructure, and high-temperature strength of TiC-added Mo–Si–B alloys. *Metallurgical and Materials Transections A*, Vol. 45, No. 3, 2014, pp. 1112–1123.
[10] Kamata, S. Y., D. Kanekon, Y. Y. Lu, N. Sekido, K. Maruyama, G. Eggeler, et al. Ultrahigh-temperature tensile creep of TiC-reinforced Mo–Si–B-based alloy. *Scientific Reports*, Vol. 8, 2018, id. 10487.
[11] Zhao, M., S. Nakayama, T. Hatakeyama, J. Nakamura, and K. Yoshimi. Microstructure, high-temperature deformability and oxidation resistance of a Ti_5Si_3-containing multiphase MoSiBTiC alloy. *Intermetallics*, Vol. 50, 2017, pp. 169–179.
[12] Hatakeyama, T., N. Sekido, and K. Yoshimi. Effect of Cr addition on microstructure and oxidation resistance of a Ti_5Si_3-containing MoSiBTiC alloy. *Corrosion Science*, Vol. 166, 2020, id. 108418.
[13] Hatakeyama, T., N. Sekido, and K. Yoshimi. Effect of Ti_5Si_3 phase on mechanical properties and oxidation resistance of MoSiBTiC-based alloys. *Journal of the Gas Turbine Society of Japan*, Vol. 46, No. 6, 2018, pp. 486–494.
[14] Burk, S., B. Gorr, M. Krüger, M. Heilmaier, and H.-J. Christ. Oxidation behavior of Mo–Si–B–(X) alloys: macro- and micro-alloying (X = Cr, Zr, La_2O_3). *JOM*, Vol. 63, No. 12, 2011, pp. 32–36.
[15] Ström, E., Y. Cao, and Y. M. Yao. Low temperature oxidation of Cr-alloyed $MoSi_2$. *Transactions of Nonferrous Metals Society China*, Vol. 17, No. 6, 2007, pp. 1282–1286.
[16] Rosales, I., H. Martinez, D. Bahena, J. Ruiz, R. Guardian, and J. Colin. Oxidation performance of Mo_3Si with Al additions. *Corrosion Science*, Vol. 51, No. 3, 2009, pp. 534–538.
[17] Yanagihara, K., K. Przybylski, and T. Maruyama. The role of microstructure on pesting during oxidation of $MoSi_2$ and Mo$(Si,Al)_2$ at 773 K. *Oxidation of Metals*, Vol. 47, No. 3–4, 1997, pp. 277–293.
[18] Dasgupta, T. and A. M. Umarji. Thermal properties of $MoSi_2$ with minor aluminum substitutions. *Intermetallics*, Vol. 15, No. 2, 2007, pp. 128–132.
[19] Dasgupta, T. and A. M. Umarji. Improved ductility and oxidation resistance in Nb and Al co-substituted $MoSi_2$. *Intermetallics*, Vol. 16, No. 6, 2008, pp. 739–744.
[20] Zhao, M., B. Xu, Y. Shao, J. Liang, S. Wu, and Y. Yan. Oxidation behavior of Mo_{ss}–Ti_5Si_3–T_2 composites at intermediate and high temperatures. *Intermetallics*, Vol. 118, 2020, id. 106702.
[21] Paswan, S., R. Mitra, and S. K. Roy. Isothermal oxidation behaviour of Mo–Si–B and Mo–Si–B–Al alloys in the temperature range of 400–800°C. *Materials Science and Engineering: A*, Vol. 424, No. 1–2, 2006, pp. 251–265.
[22] Gulbransen, E., K. Andrew, and F. Brassart. Oxidation of molybdenum 550° to 1,700°C. *Journal of The Electrochemical Society*, Vol. 110, No. 9, 1963, pp. 952–959.
[23] Cofer, C. and J. Economy. Oxidative and hydrolytic stability of boron nitride – A new approach to improving the oxidation resistance of carbonaceous structures. *Carbon,* Vol. 33, No. 4, 1995, pp. 389–395.
[24] Helmick, D. A., G. H. Meier, and F. S. Pettit. High temperature oxidation behavior of a Mo–3Si–1B(wt%) alloy. *Materials at High Temperatures*, Vol. 22, No. 3–4, 2005, pp. 293–307.
[25] Mitra, R. and V. V. Rama Rao. Elevated-temperature oxidation behavior of titanium silicide and titanium silicide-based alloy and composite. *Metallurgical and Materials Transactions A*, Vol. 29, No. 6, 1998, pp. 1665–1675.
[26] Taniguchi, S., T. Minamida, and T. Shibata. Oxidation behaviour of Ti_5Si_3 at temperatures between 1,400 and 1,700 K. *Materials Science Forum*, Vol. 251, 1997, pp. 227–234.
[27] Nan, X., M. Zhao, Y. Lu, N. Sekido, and K. Yoshimi. High-temperature oxidation behavior of a Ti_5Si_3-incorporated MoSiBTiC alloy. *Intermetallics*, Vol. 125, 2020, id. 106895.
[28] Li, X., L. Huang, S. Jiang, Y. Gao, Q. An, S. Wang, et al. Microstructure and super oxidation resistance of the network structured Ti–Al–Si coating. *Journal of Alloys and Compounds*, Vol. 807, 2019, id. 151679.
[29] Knaislová, A., P. Novák, F. Průša, M. Cabibbo, L. Jaworska, and D. Vojtěch. High-temperature oxidation of Ti–Al–Si alloys prepared by powder metallurgy. *Journal of Alloys and Compounds*, Vol. 810, 2019, id. 151895.
[30] El-Shobaky, H. G., M. Mokhtar, and A. S. Ahmed. Effect of MgO-doping on solid–solid interactions in MoO_3/Al_2O_3 system. *Thermochimica Acta*, Vol. 327, No. 1, 1999, pp. 39–46.
[31] Walczak, J. and E. Filipek. Studies on the $CrVMoO_7$–$Cr_2(MoO_4)_3$ system. *Thermochimica Acta*, Vol. 228, No. 15, 1993, pp. 127–130.
[32] Caplan, D. and M. Cohen. The volatilization of chromium oxide. *Journal of Electrochemical Society*, Vol. 108, No. 5, 1961, pp. 438–441.
[33] Maki, K., M. Shioda, M. Sayashi, T. Shimizu, and S. Isobe. Effect of silicon and niobium on oxidation resistance of TiAl intermetallics, *Materials Science and Engineering: A*, Vol. 153, No. 1–2, 1992, pp. 591–596.
[34] Wu, J. S., L. T. Zhang, F. Wang, K. Jiang, and G. H. Qiu. The individual effects of niobium and silicon on the oxidation behaviour of Ti_3Al based alloys. *Intermetallics*, Vol. 8, No. 1, 2000, pp. 19–28.